Proceedings of 15th International Marine Design Conference (IMDC-2024)
June 2-6, 2024
Amsterdam, the Netherlands

Leveraging the concept of information-theoretic entropy to improve a multi-fidelity design framework for early-stage design exploration of complex vessels

Nikoleta Dimitra Charisi[1,*], Hans Hopman[1] and Austin Kana[1]

ABSTRACT

Early-stage design exploration is crucial since most of the major design decision are locked-in and only small design modifications are possible at later stages. To assess the performance of the various design candidates while performing design exploration, there are available methods and tools of various fidelities. These methods can be combined to form a multi-fidelity (MF) framework that guarantees accuracy through the high-fidelity model and achieves faster computational speeds through low-fidelity models. The present study proposes the adoption of information-theoretic entropy to improve a MF design framework based on Gaussian Processes (GPs). Entropy quantifies the uncertainty associated with the prediction of the design space. We propose using this uncertainty metric both as a criterion to determine whether further designs should be sampled to construct a reliable approximation of the design space and as a criterion to establish in which optimization step the optimization of the covariance matrix for the MF-GPs should be performed. The approach was tested to benchmark analytical functions and to a ship design problem of an AXEfrigate. The approach holds potential in practical applications, as it aids in the determination of whether additional resources should be allocated for high-fidelity analysis to support early-stage exploration.

KEY WORDS

Early-stage design; Design exploration; Complex vessels; Multi-fidelity models; Information theory; Entropy; Gaussian Processes; Compositional kernels.

INTRODUCTION

Early-stage design of complex engineering systems is critical since it involves making the majority of key design decisions Mavris et al. (1998); Andrews (2018). These design decisions determine the overall configuration of the vessel, including main dimension selection, hull shape, and propulsion plant, among others. Committing to these decisions early in the design process results in a swift reduction of design freedom and entails a substantial overall cost allocation Mavris et al. (1998). Hence, it is crucial to perform a thorough exploration of the design space to identify trends and trade-offs, ultimately guiding well-informed design decisions.

In the initial stages of design, the primary focus is on recognizing design trends and crucial trade-offs within the broad design space Duchateau (2016). Typically, during this design stage, low-fidelity (LF) methods are employed. LF methods are

[1] Maritime and Transport Technology Department, Technical University of Delft, Delft, the Netherlands
[*] Corresponding Author: N.D.Charisi-1@tudelft.nl

Submitted: 23 February 2024, Revised: 22 April 2024, Accepted: 1 May 2024, Published: 21 May 2024
©2024 published by TU Delft OPEN Publishing on behalf of the authors. This work is licensed under CC-BY-4.0.
Conference paper, DOI: https://doi.org/10.59490/imdc.2024.874 e-ISSN: 3050-4864

computationally cheap but fall short in terms of accuracy. Thus, with such tools, it becomes feasible to evaluate a vast number of designs. For instance, when assessing motions and loads, linear methods like potential flow can be employed as LF models. Yet, in certain scenarios, LF methods prove inadequate for the following reasons: (1) LF models may fail to capture the complex physical behavior of complex engineering systems, and (2) LF methods, by their very nature, are simplifications derived from more advanced methods, simplified based on assumptions that may not apply to novel designs. When LF models fail to accurately capture the physical behavior of the system, it becomes necessary to incorporate HF analysis earlier in the design process. For example, Sapsis (2021) demonstrated the influence of nonlinearities on the seakeeping and vertical bending moment of the tumblehome hull.

A promising approach to integrating HF analysis earlier into the design process involves the creation of multi-fidelity (MF) models. In essence, MF models combine LF models with a HF model, aiming to harness the accuracy offered by the HF model while benefiting from the computational efficiency provided by the LF models. Beran et al. (2020) assert that 'analysis or design of a system is considered MF when there is synergistic use of different mathematical descriptions ... in the analysis or design procedure'. MF models have shown promise in diverse engineering fields, particularly in applications demanding computationally expensive iterations, such as design applications (e.g., Ng and Willcox (2015)), prediction of extreme loads (e.g., Drummen et al. (2022)), and solving partial differential equations (e.g., Perdikaris et al. (2017)).

In the context of information theory, entropy serves as a metric for quantifying the amount of information inherent in a message Shannon (1948). This concept can be extended to compute the information associated with an event, random variable, or probability distributions Murphy (2012). In the context of design applications, entropy can function as a metric for assessing the uncertainty associated with predicting the design space. Consequently, entropy can be utilized to enhance design exploration by quantifying such uncertainty.

Different entropy metrics have been employed to support engineering applications. Nevertheless, to the authors' best knowledge, a research gap exists in utilizing entropy to enhance a MF design framework for the early-stage design of complex vessels. Therefore, this research establishes a MF design framework and explores the role of entropy in facilitating the design exploration of complex vessels. More specifically, the utilization of entropy is proposed to determine the necessary number of HF simulations for MF design optimization. As noted by Mainini et al. (2022), a mathematical formulation to determine the required number of HF simulations for MF analysis is currently lacking. The authors suggest that entropy can be considered as a suitable mathematical formulation for this purpose. Furthermore, as an expansion of Charisi et al. (2022b), we suggest that entropy can act as an indicator to perform kernel optimization throughout the optimization process.

RELEVANT WORK

Early-stage design exploration of novel vessels with multi-fidelity models

As previously stated, the importance of early-stage design lies in the crucial decisions that shape a vessel's performance. To achieve a good design, ship designers must make well-informed decisions. This involves conducting a broad exploration of the design space, considering various concepts Van Oers et al. (2018). The goal of such exploration is to discern design trends and crucial trade-offs Andrews (2018), rather than offering highly precise values for specific key performance indicators (KPIs). The difficulty lies in striking a balance between attaining the necessary accuracy and managing computational costs, given our constraints in terms of both computation and time. When designing novel vessels, it becomes essential to incorporate HF analysis early in the process to effectively capture design trends Charisi et al. (2022a). However, achieving the required accuracy through HF tools results in escalated costs. These costs can be offset by integrating HF analysis via MF analysis.

State-of-the-art research incorporates MF analysis in ship design. In this section, characteristic examples of studies are presented, without aiming for an exhaustive literature review. The design optimization of SWATH hull forms was explored by Bonfiglio et al. (2018, 2020), who evaluated the vessel's seakeeping using two methods: a strip theory and a boundary element method based on the potential flow assumption Bonfiglio et al. (2018). Additionally, the hull forms were assessed

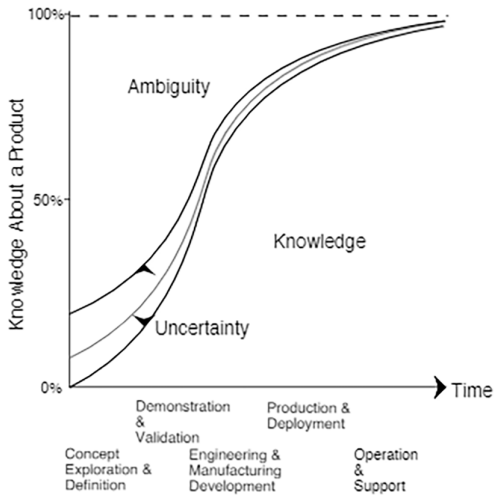

Figure 1: Variability in uncertainty across the design process Mavris et al. (1998)

for calm water resistance using a Boundary Element Method (BEM) formulated approach, assuming a potential flow-like behavior as the LF model, and a solver based on the unsteady Reynolds-averaged Navier-Stokes (RANS) equation, serving as the HF model Bonfiglio et al. (2020). The MF model was built based on GPs. Serani et al. (2022) addressed the design problem of optimizing the DTMB 5415 hull form for seakeeping and resistance. The researchers employed various analysis models, ranging from potential flow to Reynolds-Averaged Navier-Stokes equations, to solve the physical problem. Different methods were employed to construct the MF surrogates, namely stochastic radial basis functions, Kriging partial least squares, augmented expected improvement-based Kriging, and mixed-fidelity neural networks. Gaggero et al. (2022) tackled the problem optimizing a marine propeller through two methods—utilizing an inviscid potential flow-based BEM approach as the LF method and employing an inviscid finite volume RANS solver as the HF method. All the studies report promising results.

As mentioned earlier, the primary objective in early-stage design is to identify the concept that best addresses the design problem through key decisions. However, a substantial portion of relevant research, including the research studies presented, has concentrated on hull optimization, primarily emphasizing quantities of interest like resistance or seakeeping. The authors have envisioned the possibility of advancing such frameworks to earlier stages in the design process to enhance decision-making effectiveness. The uncertainty of the design space prediction is a significant factor that can be utilized to facilitate the introduction of such methods earlier on in the design process.

Uncertainty is associated with the lack of knowledge North (2017). While uncertainty is closely connected to risk, the primary distinction lies in the ability to assign a quantifiable value to risk, a task that proves challenging in the realm of uncertainty Silver (2012). Mavris et al. (1998) highlighted that there is heightened uncertainty in the early phases of the design, as shown in Figure 1. This uncertainty is introduced by the assumptions, the analysis codes of various fidelities, economic uncertainty, or technological risks. Using information-theoretic entropy as a metric enables the quantification of uncertainty in predicting the design space. In this study, the objective is to leverage this uncertainty, measured through entropy, to facilitate the early-stage design of innovative vessels.

Information theory: the entropy

According to Martignon (2001), information theory ‘is the mathematical treatment of the concepts, parameters and rules governing the transmission of messages through communication systems’. In 1948, Claude Shannon laid the foundation for information theory. The concepts and principles of information theory have expanded far beyond their original appli-

cation. Nowadays, they find application in various domains, including cryptography, machine learning, economics, and neuroscience. In the context of early-stage design, there is a direct link between design exploration and information theory via uncertainty. Krus (2013) states that 'design theory should really be a theory of design information'.

Entropy, a foundational concept in information theory, can be understood as either the measure of information content or the degree of randomness associated with a discrete random variable Duplantier and Rivasseau (2018). Various mathematical formulations exist for entropy, with some of the most commonly used ones encompassing relative entropy, or commonly known as KL divergence, and mutual information. The relevant equations to be employed in this study are presented in a subsequent section.

Entropy has found application in research problems related to design optimization. Saad and Xue (2023) proposed using entropy as a means to identify design configurations with a high likelihood of attaining optimal solutions. In such content, entropy was applied to assess the partial configuration candidates represented as branches in the AND-OR tree, aiding in the elimination of improbable branches to lead to the optimal outcome. In addition, Krus (2013) suggested that the entropy rate, which is based on Shannon's information entropy, can be a performance criterion to characterize the difficulty of different optimization problems. Farhang-Mehr and Azarm (2008) proposed an entropy-based metric to assess the quality of solution sets obtained during design optimization. The assessment is based on the distribution of the solution set over the pareto optimal frontier. Finally, Chaudhuri et al. (2020) proposed a MF design framework for risk-averse design optimization. The method is based on importance sampling and cross-entropy.

In this study, entropy serves as a metric to quantify the uncertainty within the early-stage design space. The proposal is to employ this metric as a termination criterion for concluding the design exploration process. The rationale behind this recommendation lies in the observation that, to the best of our knowledge, these problems typically operate under a predetermined budget. Thus, entropy can form a criterion to make an informed decision regarding the termination of the optimization process. Furthermore, the authors advocate for using entropy as an indicator for optimizing the covariance matrix via the optimization of the kernel function, as an extension of the method proposed in Charisi et al. (2022b). The technical details of the framework are elucidated in the following section.

PROPOSED METHOD

This section outlines the technical aspects of the methods employed in constructing the proposed framework. Specifically, it offers a comprehensive overview of the framework itself and presents the mathematical formulation of MF-GPs, compositional kernels, Bayesian optimization, and information entropy.

Proposed Framework

The flowchart illustrating the design architectural framework (DAF) is depicted in Figure 2. Organized around three primary blocks—generation, analysis, and optimization engines—the design framework shares commonalities with other design frameworks. However, the distinctive feature of this particular framework lies in the way the analysis and optimization engines are constructed to encompass the information entropy metrics. The analysis engine is dedicated to constructing the MF surrogate model for the design space. To enhance the precision of design space predictions, compositional kernels, as kernel functions, are employed to discern trends within the design space Charisi et al. (2022b). Entropy serves as a criterion for determining the optimization step where kernel optimization is most beneficial. Additionally, the optimization engine is designed to efficiently identify the optimal design point using Bayesian optimization. Entropy is incorporated into this phase of the framework as a criterion for terminating the optimization process.

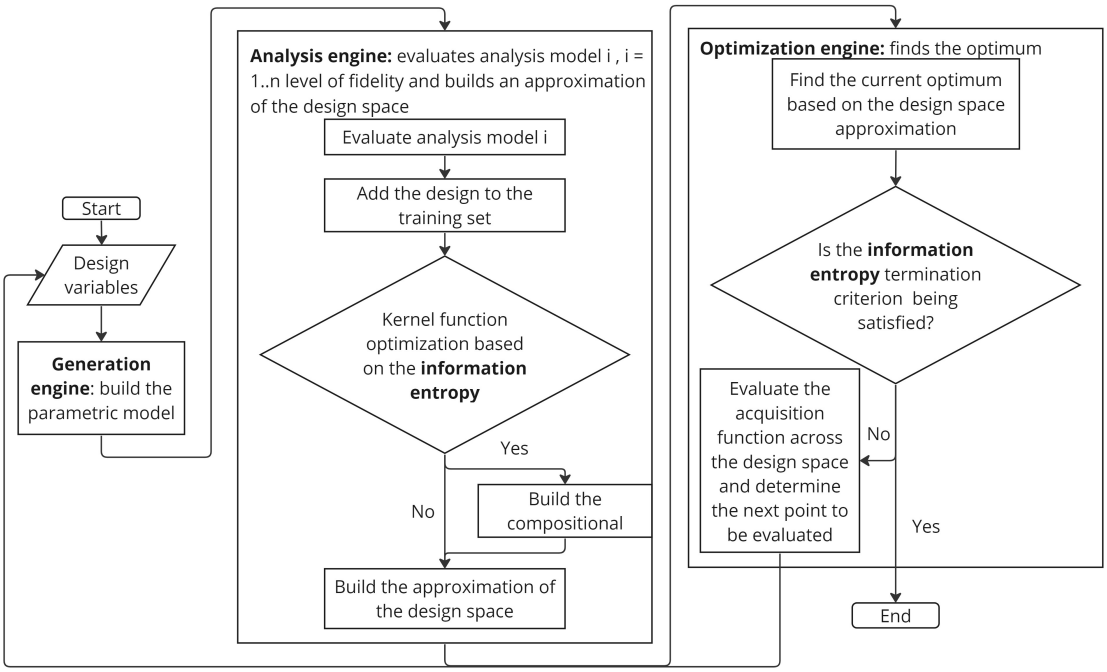

Figure 2: Flowchart of the design framework

Gaussian Processes, MF-Gaussian Processes and Compositional Kernels

Gaussian Processes

GPs are used to build approximations of real-world processes $f(x)$. Mathematically, a GP is defined as "a collection of random variables, any finite number of which have a joint Gaussian distribution, and it is fully characterized by its mean and covariance function Rasmussen (2003)". The mathematical formulation for the GPs is taken from Rasmussen (2003). The GP is fully defined by a mean $\mu(x)$ and a covariance function $k(x, x')$ according to Equations 1, 2, and 3. A common practice is to assign the prior a zero mean and a kernel function $K_{ij} = k(x_i, x_j; \theta)$.

$$f(x) \sim \mathcal{GP}(m(x), k(x, x')) \tag{1}$$

$$m(x) = \mathbb{E}[f(x)] \tag{2}$$

$$k(x, x') = \mathbb{E}[f(x) - m(x)][f(x') - m(x')] \tag{3}$$

The available analysis or experimental data can be described according to Equation **??**:

$$y = f(x) + \epsilon, \epsilon \sim \mathcal{N}(0, \sigma_{\mathrm{n}}^2 \mathcal{I}) \tag{4}$$

where f represents the function to be approximated and ϵ represents the error term which is assumed to be normally distributed with variance σ_{n}^2.

GPs are part of the Bayesian methods, where a pivotal aspect of the analysis involves the prior distribution. The prior distribution encapsulates our pre-existing knowledge or assumptions about the unknown function f. The prior distribution of the observed data X and the test data X' is determined according to Equation 5.

$$\begin{bmatrix} y \\ f_* \end{bmatrix} \sim \mathcal{N}\left(\begin{bmatrix} 0 \\ 0 \end{bmatrix}, \begin{bmatrix} K(X,X) + \sigma_{\mathrm{n}}^2 I & K(X,X_*) \\ K(X_*,X) & K(X_*,X_*) \end{bmatrix} \right) \tag{5}$$

where f_* are the function values evaluated at the test locations X_*. In Bayesian learning, the prior distribution is revised by incorporating the observed data, resulting in the formation of the predictive distribution. Mathematically, the prior distribution is conditioned on the observed data to form the predictive distribution according to Equations 6, 7, and 8:

$$f_* | X, X_*, y \sim \mathcal{N}(\mu_*, \sigma_*^2) \tag{6}$$

$$\mu_* = k_*^T (K + \sigma_{\mathrm{n}}^2 I)^{-1} y \tag{7}$$

$$\sigma_*^2 = k_{**} - k_*^T (K + \sigma_{\mathrm{n}}^2 I)^{-1} k_* \tag{8}$$

where $K = K(X,X)$, $k_{**} = k(x_*, x_*)$ and $k_* = k(x_*)$. In order to optimize the model's hyperparameters, , the marginal log-likelihood was applied. The marginal log-likelihood is defined according to Equation 9.

$$\log p(y|x,\theta) = -\frac{1}{2} \log|K + \sigma_{\mathrm{n}}^2 I| - \frac{1}{2} y^T [K + \sigma_{\mathrm{n}}^2 I]^{-1} y - \frac{n}{2} \log 2\pi \tag{9}$$

MF Gaussian Processes

The present study adopts the autoregressive scheme AR1 introduced by Kennedy and O'Hagan (2000). The scheme is based on the assumption that there is a linear dependency among different fidelity models. The mathematical formulation follows the description in Le Gratiet and Garnier (2014). The mathematical description of the bifidelity model is given since the case studies deal with bifidelity problems. The sub-models are linked according to Equation 10 and 11. The HF function connects to the LF function via a scaling function ρ and an additive function δ. It is assumed that F_2 refers to the HF function and F_1 refers to the LF function. The function δ is a GP which is independent of F_1.

$$F_2(x) = \rho(x) F_1(x) + \delta(x) \tag{10}$$

$$F_1(x) \perp \delta(x) \tag{11}$$

The predictive model is a multivariate normal distribution described by Equation 12, with a mean function according to Equation 13 and a variance according to Equation 14.

$$[F_2(x) | \boldsymbol{F} = \boldsymbol{f}, (\boldsymbol{\beta_1}, \boldsymbol{\beta_2}, \rho), (\sigma_1^2, \sigma_2^2), (\boldsymbol{\theta_1}, \boldsymbol{\theta_2})] \sim \mathcal{N}(m_{F_2}(x), s_{F_2}^2(x)) \tag{12}$$

$$m_{F_2}(x) = \mathbf{h}(x)^T \boldsymbol{\beta} + k(x)^T \boldsymbol{V}^{-1} (\boldsymbol{f} - \boldsymbol{H}\boldsymbol{\beta}) \tag{13}$$

$$s_{F_2}(x) = \rho^2 \sigma_1^2 + \sigma_2^2 - \boldsymbol{k}^T \boldsymbol{V}^{-1} \boldsymbol{k}(x) \tag{14}$$

where the trend parameters $\boldsymbol{\beta} = \begin{pmatrix} \beta_1 \\ \beta_2 \end{pmatrix}$, and $\boldsymbol{f} = \begin{pmatrix} f_1 \\ f_2 \end{pmatrix}$. The variance parameters σ_1^2, σ_2^2 and the parameters θ_1, θ_2 are the model's hyperparameters.

$$\boldsymbol{H} = \begin{pmatrix} \boldsymbol{f}_1'(x_1^{(1)}) & 0 \\ \vdots & \vdots \\ \boldsymbol{f}_1'(x_{n_1}^{(1)}) & 0 \\ \rho \boldsymbol{f}_1'(x_1^{(2)}) & \boldsymbol{f}_2'(x_1^{(2)}) \\ \vdots & \vdots \\ \rho \boldsymbol{f}_1'(x_{n_2}^{(2)}) & \boldsymbol{f}_2'(x_{n_2}^{(2)}) \end{pmatrix} \tag{15}$$

$$\boldsymbol{h}(x)^T = (\rho \boldsymbol{f}_1'(x), \boldsymbol{f}_2'(x)) \tag{16}$$

The covariance matrix is calculated as described in Equation 17.

$$\boldsymbol{V} = \begin{pmatrix} \sigma_1^2 R_1(\boldsymbol{D_1}) & \rho\sigma_1^2 R_1(\boldsymbol{D_1}, \boldsymbol{D_2}) \\ \rho\sigma_1^2 R_1(\boldsymbol{D_2}, \boldsymbol{D_1}) & \rho^2\sigma_1^2 R_1(\boldsymbol{D_2}) + \sigma_2^2 R_2(\boldsymbol{D_2}) \end{pmatrix} \tag{17}$$

Compositional Kernels

The covariance matrix conveys the degree of resemblance among data points Rasmussen (2003) and integrates prior beliefs and knowledge regarding the function f. The validity of the covariance matrix requires both symmetry and positive semi-definiteness. Prior research has examined basis functions used as kernel functions, which are defined as functions generating valid covariance matrices. For instance, the periodic kernel is employed for modeling repetitive functions. In this study, the framework introduced in Charisi et al. (2022b) was employed. The core idea was the development of compositional kernels, aiming to facilitate early-stage design analysis and optimization.

Compositional kernels, introduced by Duvenaud et al. (2013), are defined as a combination of a limited number of basis kernels through addition or multiplication. Choosing the basis kernels is intended to mathematically encapsulate the key features of the function f or, in the context of this specific research problem, the design space. The compositional kernels are built via discrete optimization. As the objective function, the Bayesian Information Criterion (BIC) was used as proposed in the original paper Duvenaud et al. (2013). BIC is defined according to Equation 18.

$$\mathcal{BIC} = k_{hyp} \ln n - 2 \ln L \tag{18}$$

where n is the number of training data, k_{hyp} is the number of hyperparameters, and L is the maximized likelihood value. BIC comprises two elements: a penalty term determined by the count of model parameters and a term derived from the likelihood function. The advantage of opting for BIC over maximizing the marginal log-likelihood is its attention to the complexity of the kernel function. By favoring functions with fewer hyperparameters, BIC aids in preventing overfitting.

Bayesian Optimization

Bayesian optimization (BO) has found extensive application in addressing optimization problems characterized by objective functions that are costly to evaluate. It comprises three fundamental components: establishing the prior distribution, refining the prior distribution to derive the posterior distribution, and determining the subsequent sampling point Brochu et al. (2009). The initial two components are associated with shaping the surrogate model, while the last one is linked to the acquisition function. The MF surrogate model in the proposed framework was built via MF-GPs as described in the previous sections. The acquisition function establishes a strategy for assessing the utility of evaluating the objective function at specific points within the search space Di Fiore and Mainini (2024). The objective of the acquisition function is to strike a

balance between exploring new areas and exploiting known areas within the search space. For this research, Expected Improvement (EI) was employed as the acquisition function, as described in Equation 19.

$$\alpha_{\text{EI}}(y_{\text{best}}, \mu.\sigma) = -\left(\phi\left(\frac{y_{\text{best}} - \mu}{\sigma}\right) + \frac{y_{\text{best}} - \mu}{\sigma} \cdot \Phi\left(\frac{y_{\text{best}} - \mu}{\sigma}\right)\right) \cdot \sigma \tag{19}$$

y_{best} represents the current optimum, μ and σ denote the mean and covariance matrix, respectively, while ϕ and Φ refer to the probability density function and the cumulative distribution function, respectively.

Information Entropy

Entropy measures the uncertainty that observers have about the state of a random variable X Varley et al. (2023). The entropy $H[p(x)]$ of a distribution $p(x)$ is a measure measuring the uncertainty in the distribution Rasmussen (2003). The integral can be replaced by a sum of discrete variables. The differential entropy for continuous variables is calculated according to Equation

$$H(X) = -\int_s f(x) \log f(x)\, dx \tag{20}$$

where S is the support of the probability density function. Regarding the multivariate Gaussian distribution, the entropy is defined according to Equation 21.

$$H[\mathcal{N}(\mu, \Sigma)] = \frac{1}{2} \log |\Sigma| + \frac{D}{2} \log 2\pi e \tag{21}$$

where D is the number of dimensions. Unlike entropy for discrete random variables, differential entropy can take negative values. The covariance matrix is guaranteed to be symmetric positive semi-definite. However, in instances where the covariance matrix becomes singular, the entropy value tends toward negative infinity. To mitigate this issue for singular matrices, the eigenvalues are computed. Any zero eigenvalues are replaced with a value of 10^{-6}, and the covariance matrix is then reconstructed based on the adjusted eigenvalues using Equation 22.

$$A = U \Lambda U^{-1} \tag{22}$$

where A represents an $n \times n$ matrix, U is an $n \times n$ matrix containing the eigenvectors of A, with each column of U representing an eigenvector of A, and Λ is an $n \times n$ diagonal matrix containing the eigenvalues of A along its diagonal elements.

The termination of the optimization loop occurs when the quantified uncertainty of the design space prediction, assessed through entropy, reaches a predetermined threshold. To ensure robustness, the criterion includes the condition that the value of entropy should not increase by more than a predetermined margin for n iterations. In summary, the formulation of the termination criterion can be found in Algorithm 1. A comparable concept was applied to the optimization criterion for compositional kernels. Entropy serves as an indicator to decide whether compositional kernel optimization should be conducted. The rationale behind this approach is that a notable decrease in entropy signifies a significant change in the predictive distribution. The formulation of the kernel optimization criterion is detailed in Algorithm 2.

input : $\Delta H_{\text{critical}}, \Delta H_{\text{margin}}, nr_{\text{iter}}^{\text{critical}}, nr_{\text{iter}}^{\text{max}}$; `/* critical value of entropy change, acceptable margin of entropy change, critical number of optimization iterations, maximum number of optimization iterations */`

output: $\epsilon_x, \epsilon_f, \epsilon_t, \text{RMSE}, nr_{\text{iter}}^{\text{terminate}}$; `/* performance, metrics, step to terminate the optimization loop */`

$nr_{\text{iter}}^{i} \leftarrow 1$;
$comp_cost \leftarrow 0$;
$counter \leftarrow 0$;
while $nr_{\text{iter}}^{i} \leq nr_{\text{iter}}^{\text{max}}$ **do**
  Compute μ, σ from Equations 7, 8 ; `/* MF surrogate model */`
  Compute entropy H_{iter_i} from Equation 21;
  if $nr_{\text{iter}}^{i} = 1$ **then**
    $H_0 \leftarrow H_{iter_i}$; `/* Reference entropy value */`
  end
  else
    if $H_{iter_i} > H_0$ **then**
      $H_0 \leftarrow H_{iter_i}$
    end
  end
  Compute $comp_cost_i$;
  $comp_cost \leftarrow comp_cost + comp_cost_i$; `/* Computational cost */`
  Compute $\epsilon_x, \epsilon_f, \epsilon_t$, RMSE from Equations 24,25,26,23; `/* Performance metrics */`
  if $H_0 - H_{iter_i} \geq \Delta H_{\text{critical}}$ **then**
    $counter \leftarrow counter + 1$; `/* Counting optimization steps */`
    if $counter = nr_{\text{iter}}^{\text{critical}}$ **then**
      $nr_{\text{iter}}^{\text{terminate}} = nr_{\text{iter}}^{i}$;
      break;
    end
  end
  if $H_{iter_i} - H_{iter_i - 1} \geq \Delta H_{\text{margin}}$ **then**
    $counter \leftarrow 0$
  end
  $nr_{\text{iter}}^{i} \leftarrow nr_{\text{iter}}^{i} + 1$;
end

Algorithm 1: Termination criterion

input : $\Delta H_{\text{critical}}, \Delta H_{\text{margin}}, nr_{\text{iter}}^{\text{max}}, nr_{\text{iter}}^{\text{critical}}$; `/* critical value of entropy change, acceptable margin of entropy change, maximum number of optimization iterations, critical number of optimization iterations */`

output: $\epsilon_x, \epsilon_f, \epsilon_t$, RMSE; `/* performance, metrics */`

$nr_{\text{iter}}^{i} \leftarrow 1$;
$bool_{ker_opt} \leftarrow$ False ;
$counter \leftarrow 0$;
while $nr_{\text{iter}}^{i} \leq nr_{\text{iter}}^{\text{max}}$ **do**
  Compute μ, σ from Equations 7, 8 ; `/* MF surrogate model */`
  Compute entropy H_{iter_i} from Equation 21;
  if $nr_{\text{iter}}^{i} = 1$ **then**
    $H_0 \leftarrow H_{iter_i}$; `/* Reference entropy value */`
  end
  Compute $\epsilon_x, \epsilon_f, \epsilon_t$, RMSE from Equations 24,25,26,23; `/* Performance metrics */`
  if $|H_0 - H_{iter_i}| \geq \Delta H_{\text{critical}}$ **and** $(H_0 - H_{iter_i})(H_0 - H_{iter_i - 1}) > 0$ **then**
    $counter \leftarrow counter + 1$; `/* Counting optimization steps */`
    if $counter = nr_{\text{iter}}^{\text{critical}}$ **then**
      Perform compositional kernels optimization;
      $H_0 \leftarrow H_{iter_i}$;
    end
  end
  if $|H_{iter_i} - H_{iter_i - 1}| \geq \Delta H_{\text{margin}}$ **and** $(H_{iter_i} - H_0)(H_{iter_i} - H_{iter_i - 1}) < 0$ **then**
    $counter \leftarrow 0$
  end
  $nr_{\text{iter}}^{i} \leftarrow nr_{\text{iter}}^{i} + 1$;
end

Algorithm 2: Kernel optimization criterion

Error metrics

Various error metrics were employed to evaluate the accuracy of the proposed framework. The Root Mean Squared Error (RMSE), as defined in Equation 23, was used to quantify the accuracy of the models in predicting the design space. Furthermore, the error metrics ϵ_x, ϵ_f, ϵ_t characterize the normalized error in the design space, the objective function, and the Euclidean distance in the normalized x-f hyperspace. Detailed descriptions of these metrics are provided in Equations 24, 25, and 26.

$$\varepsilon_{RMSE} = \frac{1}{y_{max} - y_{min}} \sqrt{\frac{1}{N} \sum_{i=1}^{N} (y_i - \hat{y}_i)^2} \tag{23}$$

$$\epsilon_x = \frac{\|\hat{x}^* - x^*\|}{\sqrt{N}} \tag{24}$$

$$\epsilon_f = \frac{f(\hat{x}^*) - f_{\text{min}}}{f_{\text{max}} - f_{\text{min}}} \tag{25}$$

$$\epsilon_t = \sqrt{\frac{\epsilon_x^2 + \epsilon_f^2}{2}} \tag{26}$$

CASE STUDIES

The case studies encompass a simplified example, using the Jump Forrester function, to illustrate the rationale behind integrating information entropy into an early-stage design framework. Subsequently, two analytical problems will the addressed: the 1D Heterogeneous function and the 2D shifted rotated Rastrigin function. Finally, a realistic ship design is showcased, addressing the 2D design of the AXE frigates focused on optimizing the wave-induced vertical bending moment (VBM).

A toy example: the Jump Forrester function

This simplified design problem aims to give a better understanding on how and why entropy is integrated in the design framework. The toy case study assumes a one-dimensional design space characterized by the Jump Forrester function as described in Equations 27 and 28. The initial dataset comprises 5 HF and 35 LF observations.

$$f_1(x) = \begin{cases} (6x-2)^2 \sin(12x-4), & 0 \leq x < 0.5 \\ (6x-2)^2 \sin(12x-4) + 10, & 0.5 \leq x \leq 1 \end{cases} \tag{27}$$

$$f_2(x) = \begin{cases} 0.5 f_1(x) + 10(x-0.5) - 5, & 0 \leq x < 0.5 \\ 0.5 f_1(x) + 10(x-0.5) - 2, & 0.5 \leq x \leq 1 \end{cases} \tag{28}$$

Figure 3 illustrates the evolution of error metrics and entropy throughout the optimization process. Evidently, an augmented

dataset correlates with heightened accuracy in the obtained results. This is a general trend which can be observed in both the evolution of H and ϵ throughout the optimization. Figure 3a illustrates a notable decrease in entropy between iteration 10 and 11. The decrease in entropy is correlated with a reduction in the error metrics, as depicted in Figure 3b. It is evident that the variations in entropy do not perfectly align with changes in the error metrics. This underscores the importance of treating entropy as an indicator rather than an absolute measure.

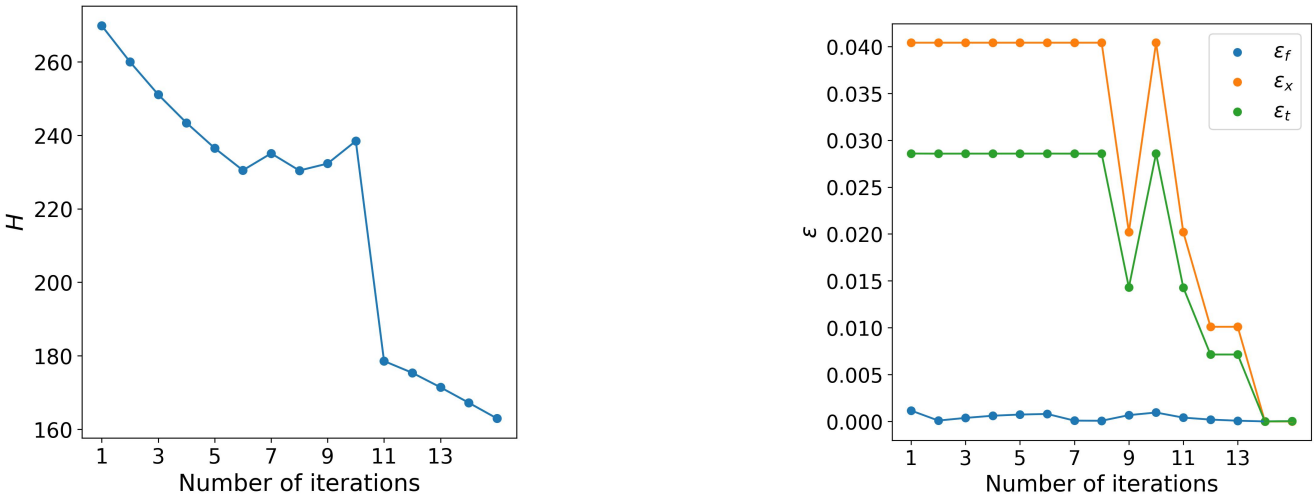

(a) Tracking H throughout the optimization iterations

(b) Tracking ϵ throughout the optimization iterations

Figure 3: Comparing H with ϵ error metrics

To further analyze the results, the design spaces for iterations 9, 10, and 11 are plotted in Figure4. Specifically, Figure 4a displaying the prediction of the design space at step 9, reveals that the prediction is inaccurate across the domain and the variance is high. However, the area where the optimum lies is further explored, resulting in a lower calculated error. This localized behavior cannot be captured via entropy which is calculated over the entire design domain. Similarly, the design space in iteration 10, depicted in Figure 4b, is characterized by an inaccurate prediction of the design space and high uncertainty bounds. Entropy is slightly increased between iteration 9 and 10. In addition, the measured error is higher since the prediction fails to capture the area containing the optimum. Moving on to iteration 11, illustrated in Figure 4c, the prediction aligns more closely with the true design space, resulting in a significant reduction in both calculated error and entropy.

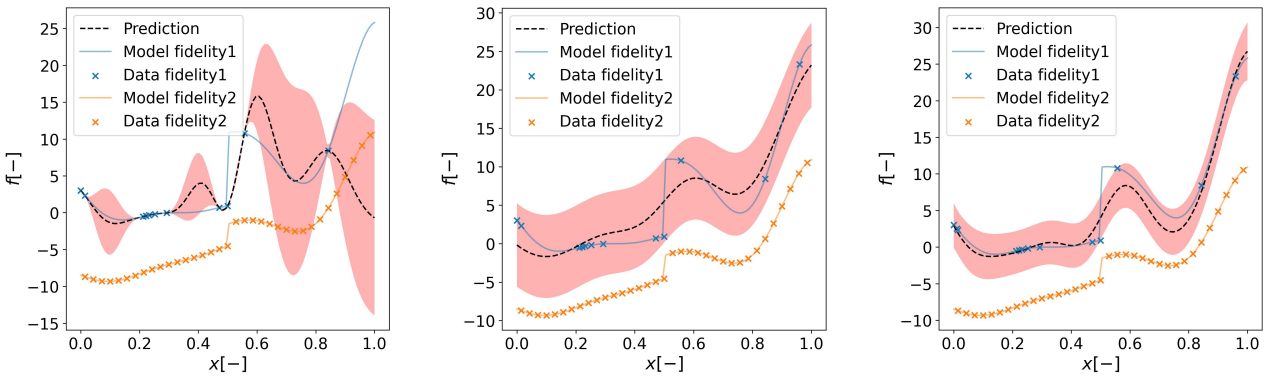

(a) Optimization Step 9

(b) Optimization Step 10

(c) Optimization Step 11

Figure 4: Design space for various optimization steps

Analytical function 1D: the Heterogeneous function

A commonly employed analytical function is the Heterogeneous function, known for its localized and multi-modal behavior Mainini et al. (2022). The 1D Heterogeneous function is described by the Equations 29 and 30. The Heterogeneous function can be visualized in Figure 5.

$$f_1(x) = \sin 30(x-0.9)^4 \cos 2(x-0.9) + (x-0.9)/2 \tag{29}$$

$$f_2(x) = (f_1(x) - 1.0 + x)/(1.0 + 0.25x) \tag{30}$$

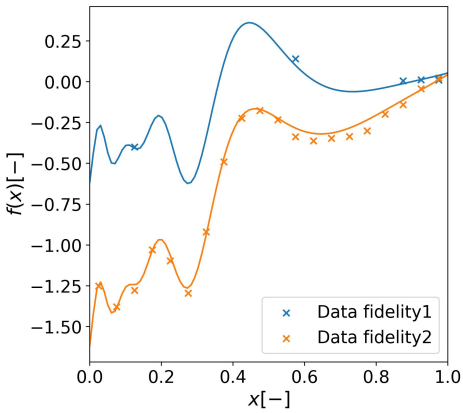

Figure 5: Heterogeneous function

where $0 \leq x \leq 1$. In this case study, the initial training set comprised included 10 HF data fused with 35 LF data. The base case underwent 15 optimization steps. The parameters of this case study remained consistent when evaluating both the entropy-driven termination criterion and entropy-driven kernel optimization. Furthermore, recognizing the substantial impact of the training set on model performance, statistical insights were derived by employing 20 distinct training sets in both scenarios.

Regarding the entropy-driven optimization criterion, relevant statistics can be found in Tables 1 and 2 for the proposed and the base model, respectively. Six scenarios were examined, involving the increase of noise in the training data from 0.00 to 0.05. The comparison of mean error metric values is presented and visualized in Figure 6. The main observation is that, as anticipated, the error generally rises with an increase in noise level. In most instances, the proposed model demonstrates comparable or slightly elevated errors compared to the base model, while concurrently achieving significant computational savings. For instance, when $\sigma_n = 0.04$, the average number of iterations is 10.5, resulting in a 30% improvement compared to the 15 iterations in the base scenario.

Regarding the entropy-driven kernel optimization, the results can be found in Tables Tables 3 and 4 for the proposed and base models, respectively. The visualization of mean error metrics is presented in Figure 7. As illustrated in Figure 7, the proposed model demonstrates a comparable performance to the base model, and their results are closely aligned, thus the performance of the two models is similar.

Analytical function 2D: the Shifted Rotated Rastrigin function

In this case study, the 2D shifted-rotated Rastrigin function was employed. This function is characterized by multi-modal behavior. To investigate this, a noise term e_{data} was added to the 2D shifted-rotated Rastrigin function, taken from Mainini et al. (2022). Thus, for this analysis, Equations 31 and 34 were used. The function can be visualized in Figure 8.

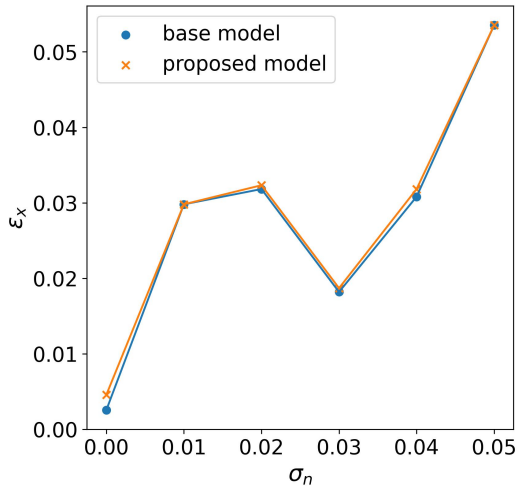

(a) Graph depicting the relationship between ϵ_x and σ_n

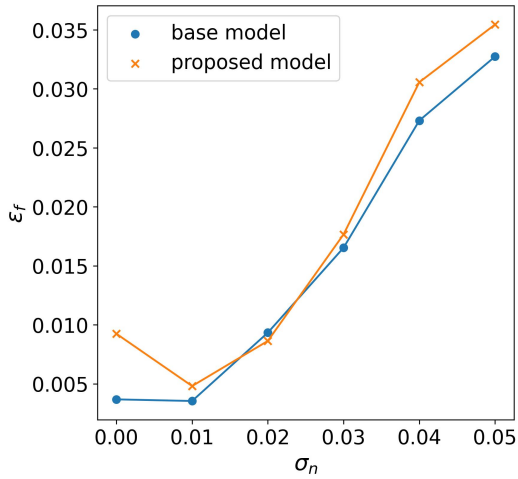

(b) Graph depicting the relationship between ϵ_f and σ_n

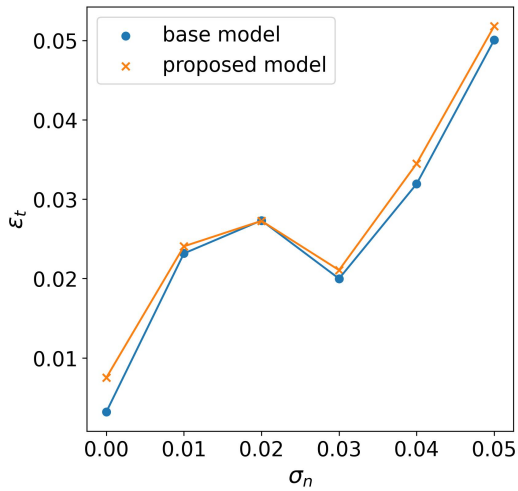

(c) Graph depicting the relationship between ϵ_t and σ_n

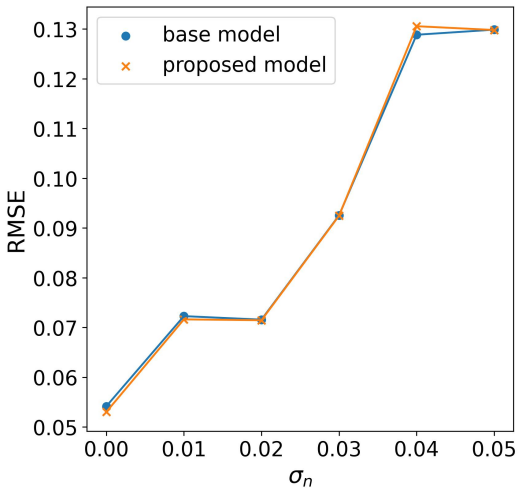

(d) Graph depicting the relationship between $RMSE$ and σ_n

Figure 6: Heterogeneous function: Entropy-driven termination criterion, while varying the noise σ_n

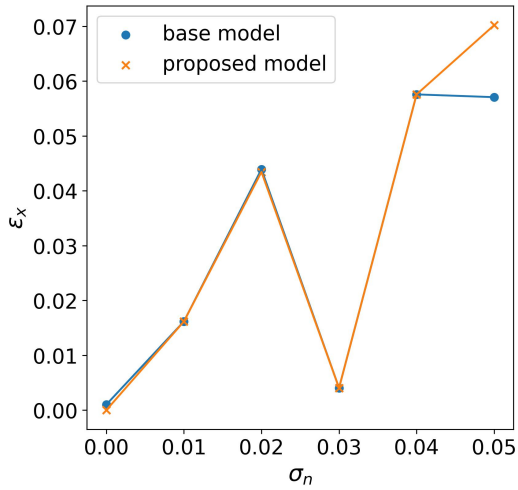

(a) Graph depicting the relationship between ϵ_x and σ_n

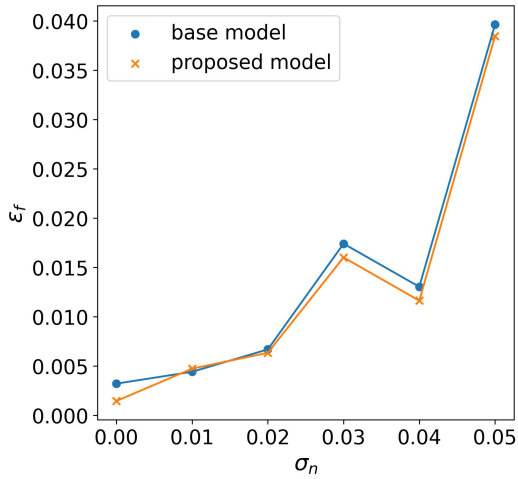

(b) Graph depicting the relationship between ϵ_f and σ_n

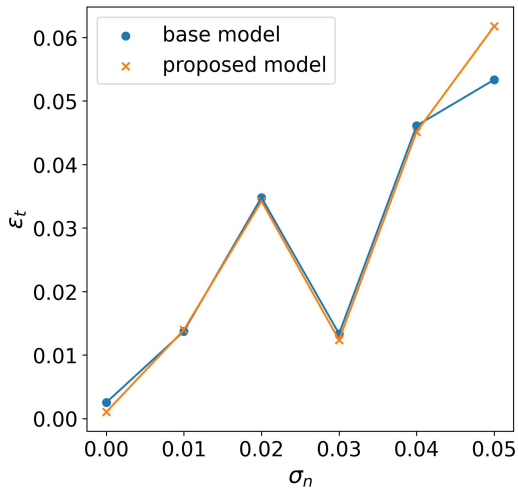

(c) Graph depicting the relationship between ϵ_t and σ_n

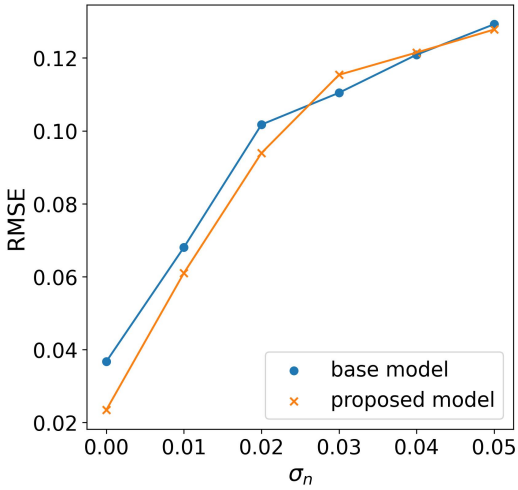

(d) Graph depicting the relationship between $RMSE$ and σ_n

Figure 7: Heterogeneous function: Entropy-driven kernel optimization, while varying the noise σ_n

Table 1: Proposed model performance (entropy-driven termination criterion, Heterogeneous function)

σ_n	ϵ_x **(std)**	ϵ_f **(std)**	ϵ_t **(std)**	$RMSE$ **(std)**	**computational cost (std)**	**optimization steps (std)**
0	0.0045 (0.0050)	0.0092 (0.0104)	0.0075 (0.0079)	0.0530 (0.0387)	2.21 (0.71)	10.45 (4.00)
0.01	0.0298 (0.0811)	0.0048 (0.0062)	0.0241 (0.0564)	0.0716 (0.0231)	2.91 (0.39)	14.5 (2.18)
0.02	0.0323 (0.0803)	0.0086 (0.0131)	0.0273 (0.0559)	0.0715 (0.0126)	2.6 (0.74)	12.75 (4.11)
0.03	0.0187 (0.0585)	0.0177 (0.0223)	0.0211 (0.0430)	0.0925 (0.0222)	2.38 (0.97)	11.6 (5.31)
0.04	0.0318 (0.0772)	0.0306 (0.0408)	0.0345 (0.06)	0.1306 (0.0528)	2.18 (1.03)	10.5 (5.62)
0.05	0.0535 (0.0991)	0.0354 (0.0362)	0.0518 (0.0703)	0.1298 (0.0485)	2.67 (0.79)	13.2 (4.29)

Table 2: Base model performance (entropy-driven termination criterion, Heterogeneous function)

σ_n	ϵ_x **(std)**	ϵ_f **(std)**	ϵ_t **(std)**	$RMSE$ **(std)**	**computational cost**	**optimization steps**
0	0.0025 (0.0044)	0.0037 (0.0062)	0.0032 (0.0053)	0.0542 (0.0516)	3	15
0.01	0.0298 (0.0811)	0.0035 (0.0024)	0.0232 (0.0566)	0.0723 (0.0230)	3	15
0.02	0.0318 (0.0804)	0.0093 (0.0130)	0.0273 (0.0559)	0.0716 (0.0126)	3	15
0.03	0.0182 (0.0586)	0.0165 (0.0217)	0.02 (0.0431)	0.0925 (0.0223)	3	15
0.04	0.0308 (0.0776)	0.0273 (0.0410)	0.0319 (0.0606)	0.1288 (0.0512)	3	15
0.05	0.0535 (0.0991)	0.03273 (0.0376)	0.05 (0.0713)	0.1299 (0.0486)	3	15

$$f_1(z) = \sum_{i=1}^{D=2} (Z_i^2 + 1 - \cos(10\pi z_i)) \tag{31}$$

where

$$z = R(\theta)(x - x*) \tag{32}$$

$$R(\theta) = \begin{bmatrix} \cos\theta & -\sin\theta \\ \sin\theta & \cos\theta \end{bmatrix} \tag{33}$$

where $x_i \epsilon [-0.1, 0.2]$ for $i = 1, .., D$, R is the rotation matrix, and $\theta = 0.2$.

$$f_2(z, \phi_i) = f_1(z) + e_r(z, \phi_i) + e_{data} \tag{34}$$

where the resolution error e_r is defined according to Equation 35.

$$e_r(z, \phi_i) = \sum_{i=1}^{D=2} \alpha(\phi) \cos^2(w(\phi) z_i + \beta\phi + \pi) \tag{35}$$

Table 3: Proposed model performance (entropy-driven kernel optimization, Heterogeneous function)

σ_n	ϵ_x **(std)**	ϵ_f **(std)**	ϵ_t **(std)**	$RMSE$ **(std)**
0	0.0 (0.0)	0.0015 (0.0030)	0.0010 (0.0021)	0.0235 (0.0279)
0.01	0.0162 (0.0590)	0.0047 (0.0047)	0.01396 (0.0412)	0.0610 (0.0218)
0.02	0.0434 (0.0964)	0.0063 (0.0059)	0.0342 (0.0668)	0.0939 (0.0618)
0.03	0.0040 (0.0049)	0.0160 (0.0131)	0.0124 (0.0091)	0.1154 (0.0633)
0.04	0.0576 (0.1077)	0.0116 (0.0081)	0.0452 (0.0743)	0.1215 (0.0468)
0.05	0.0702 (0.1114)	0.0385 (0.0562)	0.0618 (0.0847)	0.1278 (0.0529)

Table 4: Base model performance (entropy-driven kernel optimization, Heterogeneous function)

σ_n	ϵ_x **(std)**	ϵ_f **(std)**	ϵ_t **(std)**	$RMSE$ **(std)**
0	0.0010 (0.0030)	0.0032 (0.0052)	0.0025 (0.0042)	0.0367 (0.0359)
0.01	0.01616 (0.0590)	0.0044 (0.0050)	0.0137 (0.0413)	0.0681 (0.0172)
0.02	0.0439 (0.0962)	0.0067 (0.0059)	0.0348 (0.0665)	0.1017 (0.0665)
0.03	0.0040 (0.0049	0.0174 (0.0141)	0.01334 (0.0097)	0.1105 (0.0557)
0.04	0.0576 (0.1077)	0.0130 (0.0086)	0.0461 (0.0738)	0.1209 (0.0451)
0.05	0.0571 (0.1018)	0.0396 (0.0558)	0.0534 (0.0794)	0.1293 (0.0522)

with $\alpha(\phi) = \Theta(\phi)$, $w(\phi) = 10\pi\Theta$, $\beta(\phi) = 0.5\pi\Theta(\phi)$, $\Theta(\phi) = 1 - 0.0001\phi$. For the present case study, we chose $\phi = 2500$.

In this case study, the initial training set consisted of 10 HF data combined with 50 LF data. The base case underwent 15 optimization steps. Consistent with other studies, parameters were maintained constant during the assessment of both the entropy-driven termination criterion and entropy-driven kernel optimization. Statistical insights were obtained by using 20 different training sets in both scenarios.

Regarding the entropy-driven optimization criterion, relevant statistics can be found in Tables 5 and 6. The visualization of mean error metrics is presented in Figure 9. A notable observation is that, similar trends to the previous case study are observed, where the suggested model displays errors that are comparable or slightly higher than those of the base model, yet it concurrently realizes computational savings. The discrepancy between the models is more apparent, possibly due to the increased complexity of this problem. Notably, in this instance, the error does not escalate with the noise level.

Regarding the entropy-driven kernel optimization, the results can be found in Tables Tables 7 and 8 for the proposed and base models, respectively. The visualization of mean error metrics is presented in Figure 10. The findings indicate a substantial enhancement in error metrics of the proposed model compared to the base case across various scenarios. These results are noteworthy, with a more pronounced improvement compared to the previous case study. This heightened improvement could be attributed to the increased complexity of the problem or the ability of compositional kernels to better capture the structure of the function.

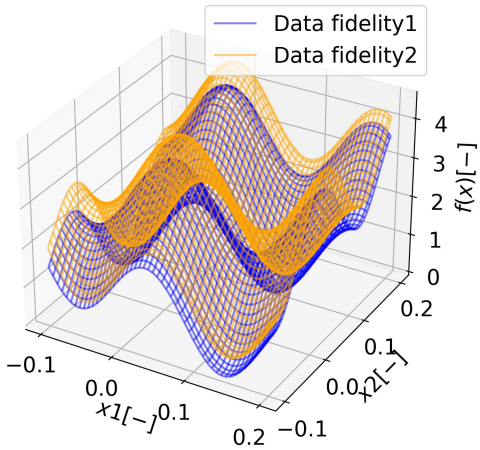

Figure 8: Rastrigin function

Table 5: Proposed model performance (entropy-driven termination criterion, Rastrigin function)

σ_n	ϵ_x **(std)**	ϵ_f **(std)**	ϵ_t **(std)**	$RMSE$ **(std)**	**computational cost (std)**	**optimization steps (std)**
0	0.1192 (0.2064)	0.0068 (0.0103)	0.0875 (0.1443)	0.1110 (0.0386)	0.9 (0.0696)	14.15 (1.53)
0.01	0.2007 (0.2475)	0.0151 (0.0207)	0.1464 (0.1722)	0.1212 (0.0570)	0.8969 (0.0845)	14.15 (1.74)
0.02	0.0239 (0.1042)	0.0035 (0.0082)	0.0192 (0.0733)	0.1094 (0.0348)	0.8875 (0.1129)	14 (2.17)
0.03	0.1044 (0.2121)	0.0097 (0.0196)	0.0775 (0.1489)	0.1538 (0.0718)	0.8844 (0.1330)	13.9 (2.45)
0.04	0.0717 (0.1706)	0.0049 (0.0093)	0.0528 (0.1199)	0.0997 (0.0351)	0.9031 (0.0850)	14.15 (1.68)
0.05	0.1924 (0.2658)	0.0121 (0.0298)	0.1367 (0.1889)	0.1312 (0.0658)	0.8875 (0.0980)	13.8 (1.91)

Ship design problem 2D: the AXE frigates

The AXE frigates are characterized by the inclusion of an AXE bow, a design initially conceived by Keuning et al. (2015). The AXE bow offers the potential to enhance a vessel's seakeeping capabilities, making it a compelling choice for frigates that must effectively carry out missions even in challenging weather conditions. The key performance indicator (KPI) for this design problem focuses on predicting the wave-induced VBM.

The VBM emerges as a significant load with substantial implications for ship structural design. It results from the uneven distribution of water pressure and gravity, resulting in the bending of the elastic hull structure Molland (2008). Wave loading conditions are assessed independently for each design variation. More specifically, we have chosen to examine the vessel in a sea state that maximizes wave-induced VBM, specifically when the wavelength equals the ship's length. Consequently, a regular sea state is selected and characterized by Equations 36 and 37 Tupper (2004). The vessel's speed was set to 0 knots. The problem is simplified into a 2D case, where only the vessel's length (L_{pp}) and breadth (B) are varied.

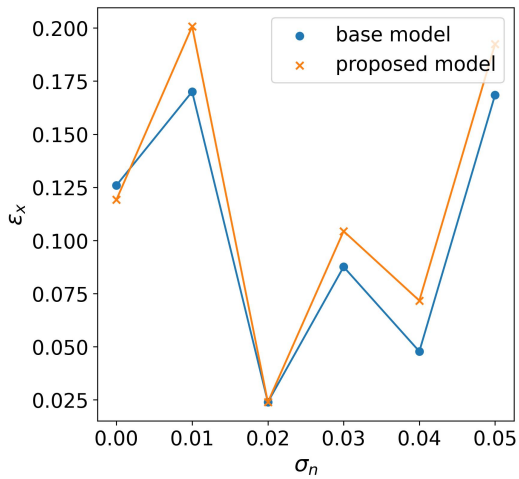

(a) Graph depicting the relationship between ϵ_x and σ_n

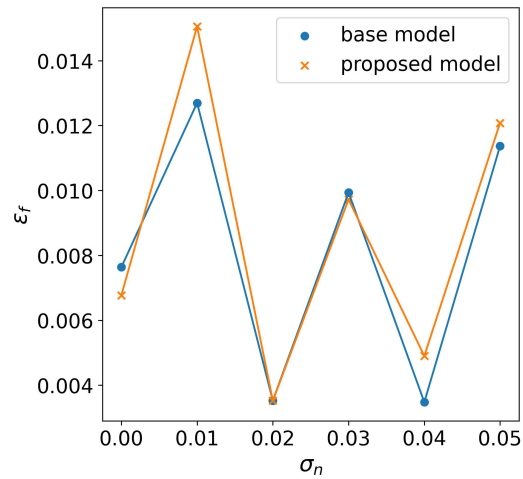

(b) Graph depicting the relationship between ϵ_f and σ_n

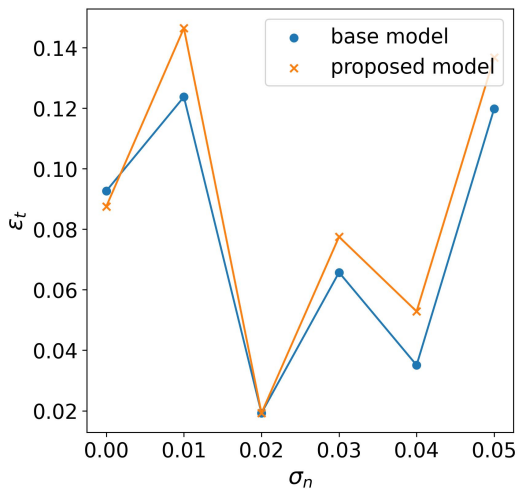

(c) Graph depicting the relationship between ϵ_t and σ_n

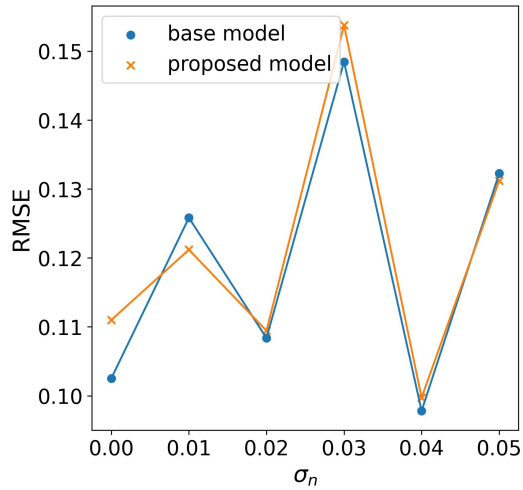

(d) Graph depicting the relationship between $RMSE$ and σ_n

Figure 9: Rastrigin function: Entropy-driven termination criterion, while varying the noise σ_n

$$\lambda = L_{pp} \tag{36}$$

$$H = 0.607 \cdot \sqrt{Lpp} \tag{37}$$

In the frequency domain (FD) calculation of the wave-induced VBM, PRECAL software, developed by Marin, was employed. PRECAL is a dedicated tool designed to predict linear responses through potential flow calculations. The tool operates by: (1) dividing the wetted hull into multiple quadrilateral panels and defining flexural modes, (2) calculating hydrodynamic coefficients through solving the linearized boundary value problem, and (3) determining ship motions and loads using linearized potential flow. Additionally, it incorporates adjustments for viscous damping based on empirical corrections.

Furthermore, the time domain (TD) results were obtained using PRETTI_R, a 3D time-domain nonlinear seakeeping and hydroelasticity tool. In contrast to PRECAL, PRETTI_R is specifically crafted for predicting motions in high sea states, en-

Table 6: Base model performance (entropy-driven termination criterion, Rastrigin function)

σ_n	ϵ_x **(std)**	ϵ_f **(std)**	ϵ_t **(std)**	$RMSE$ **(std)**	**computational cost (std)**	**optimization steps (std)**
0	0.1259 (0.2200)	0.0076 (0.0104)	0.0926 (0.1536)	0.1025 (0.0324)	0.9375 (0.0)	15 (0.0)
0.01	0.1700 (0.2320)	0.0127 (0.0209)	0.1237 (0.1623)	0.1258 (0.0557)	0.9375 (0.0)	15 (0.0)
0.02	0.0239 (0.1042)	0.0035 (0.0082)	0.0192 (0.0733)	0.1084 (0.0344)	0.9375 (0.0)	15 (0.0)
0.03	0.0876 (0.2109)	0.0099 (0.0196)	0.0657 (0.1483)	0.1485 (0.0718)	0.9375 (0.0)	15 (0.0)
0.04	0.0478 (0.1434)	0.0035 (0.0082)	0.0351 (0.1011)	0.0978 (0.0326)	0.9375 (0.0)	15 (0.0)
0.05	0.1685 (0.2606)	0.0114 (0.0299)	0.1198 (0.1852)	0.1323 (0.0643)	0.9375 (0.0)	15 (0.0)

Table 7: Proposed model performance (entropy-driven kernel optimization, Rastrigin function)

σ_n	ϵ_x **(std)**	ϵ_f **(std)**	ϵ_t **(std)**	$RMSE$ **(std)**
0	0.0902 (0.2177)	0.0076 (0.0183)	0.0663 (0.1536)	0.1070 (0.0597)
0.01	0.7382 (0.2700)	0.0150 (0.0288)	0.1245 (0.1912)	0.1349 (0.0691)
0.02	0.1115 (0.2262)	0.0096 (0.0254)	0.0796 (0.1607)	0.1175 (0.0437)
0.03	0.0543 (0.1643)	0.0015 (0.0039)	0.0389 (0.1160)	0.0961 (0.0189)
0.04	0.0756 (0.1699)	0.0035 (0.0069)	0.0540 (0.1200)	0.1043 (0.0529)
0.05	0.1050 (0.2132)	0.0069 (0.0138)	0.0759 (0.1503)	0.1012 (0.0494)

compassing rigid-body motion, elastic deformation, and hydrodynamic loads. It is also capable of considering slamming and whipping loads. Developed as part of the Cooperative Research Ships (CRS) initiative, this software calculates the Froude Krylov force by integrating incident wave hydrodynamics and hydrostatic pressure across the vessel's hull surface. The diffraction force is estimated by scaling the FD diffraction force Response Amplitude Operator (RAO) with the incident wave amplitude. The radiation force is computed through a convolution integral involving an impulse function, and slamming force can be assessed using either the Generalized Wagner Model or the Modified Logvinovich Model. PRETTI_R utilizes FD results to derive the required impulse functions.

The initial training set consists of 2 HF PRETTI_R simulations (TD data) and 20 PRECAL simulations (LF data). The LF and the HF design space can be visualized in Figure 11. The optimization steps were configured to be 10. The outcomes are presented in Tables 9 and 10 for the entropy-driven termination criterion and kernel optimization, respectively. The data was gathered through 20 simulations utilizing various initial Design of Experiments (DoEs). In general, the results exhibit similar trends to previous case studies. The performance metrics of the proposed model slightly surpass those of the base model, with an associated reduction in computational steps to an average of 8.55 from the set 10 steps. Concerning the kernel optimization scenario, the performance metrics of the proposed model are improved compared to the base model.

Table 8: Base model performance (entropy-driven kernel optimization, Rastrigin function)

σ_n	ϵ_x **(std)**	ϵ_f **(std)**	ϵ_t **(std)**	$RMSE$ **(std)**
0	0.1377 (0.2432)	0.0087 (0.0181)	0.1001 (0.1709)	0.1178 (0.0571)
0.01	0.1966 (0.2743)	0.0217 (0.0364)	0.1424 (0.1938)	0.1615 (0.0710)
0.02	0.1932 (0.2682)	0.0135 (0.0273)	0.1382 (0.1897)	0.1396 (0.0570)
0.03	0.1260 (0.2223)	0.0096 (0.0212)	0.0912 (0.1570)	0.1086 (0.0494)
0.04	0.1036 (0.2117)	0.0140 (0.0765)	0.0765 (0.1468)	0.1468 (0.0703)
0.05	0.1528 (0.2366)	0.0081 (0.0141)	0,1098 (0.1666)	0.1131 (0.0524)

Table 9: Models' performance (entropy-driven termination criterion, AXE frigates)

model	ϵ_x **(std)**	ϵ_f **(std)**	ϵ_t **(std)**	$RMSE$ **(std)**	**optimization steps (std)**
base	0.0 (0.0)	0.0436 (0.0285)	0.0308 (0.0202)	0.1300 (0.0405)	10 (0)
proposed	0.0068 (0.0172)	0.0513 (0.0304)	0.0376 (0.0232)	0.1388 (0.0416)	8.55 (2.5)

CONCLUSIONS

In summary, the paper proposes the integration of entropy, a mathematical concept from information theory, to improve a MF design framework for early-stage design exploration. Two concepts, namely the entropy-driven termination criterion and entropy-driven kernel optimization, were formulated and illustrated. The case studies encompassed analytical benchmark problems, including the 1D Jump Forrester and the 2D Shifted Rotated Rastrigin function, along with a 2D physical problem involving AXE frigate design where variations in L and B were considered.

Similar patterns were observed across the different case studies. Concerning the termination criterion, the performance metrics slightly exceeded those of the base model while concurrently achieving computational savings. This suggests the potential for a potent tool in design exploration, particularly when the goal is to discern design trends. Furthermore, the outcomes related to kernel optimization exhibited enhancements in most cases and comparable results in others. This underscores the concept's potential in integrating compositional kernels within a design optimization loop.

The inclusion of entropy in design exploration is rooted in the concept that entropy can serve as an indicator of how comprehensively the design space has been investigated. It is crucial to emphasize that entropy is not presumed to be an absolute performance measure akin to error metrics. Instead, its significance lies in the fact that in practical design exploration problems, calculating error metrics is not feasible. To advance this concept, exploring its scalability to higher-dimensional problems is an area that needs further research. Additionally, determining the critical parameters for the method is a case-dependent and challenging aspect in real-world applications.

CONTRIBUTION STATEMENT

Nikoleta Dimitra Charisi: Conceptualization; methodology; writing – original draft. **Hans Hopman:** supervision; writing – review and editing. **Austin Kana:** supervision; writing – review and editing.

Table 10: Models' performance (entropy-driven kernel optimization, AXE frigates)

model	ϵ_x **(std)**	ϵ_f **(std)**	ϵ_t **(std)**	$RMSE$ **(std)**
base	0.0 (0.0)	0.0349 (0.0298)	0.0247 (0.0210)	0.1295 (0.0523)
proposed	0.0 (0.0)	0.0180 (0.0301)	0.0127 (0.0213)	0.1133 (0.0303)

ACKNOWLEDGEMENTS

This publication is part of the project "Multi-fidelity Probabilistic Design Framework for Complex Marine Structures" (project number TWM.BL.019.007) of the research program "Topsector Water & Maritime: the Blue route" which is (partly) financed by the Dutch Research Council (NWO). The authors thank DAMEN, the Netherlands Defence Materiel Organisation (DMO), and MARIN for their contribution to the research.

REFERENCES

Andrews, D. (2018). The Sophistication of Early Stage Design for Complex Vessels. *International Journal of Maritime Engineering*, Vol 160(SE 18).

Beran, P. S., Bryson, D. E., Thelen, A. S., Diez, M., and Serani, A. (2020). Comparison of multi-fidelity approaches for military vehicle design. *AIAA AVIATION 2020 FORUM*, 1 PartF:1–34.

Bonfiglio, L., Perdikaris, P., and Brizzolara, S. (2020). Multi-fidelity Bayesian optimization of SWATH hull forms. *Journal of Ship Research*, 64(2):154–170.

Bonfiglio, L., Perdikaris, P., Vernengo, G., De Medeiros, J., and Karniadakis, G. (2018). Improving SWATH seakeeping performance using multi-fidelity Gaussian process and Bayesian optimization. *Journal of Ship Research*, 62(4):223–240.

Brochu, E., Cora, M., and De Freitas, N. (2009). A Tutorial on Bayesian Optimization of Expensive Cost Functions, with Application to Active User Modeling and Hierarchical Reinforcement Learning. Technical report, Department of Computer Science, University of British Columbia.

Charisi, N. D., Hopman, H., and Kana, A. (2022a). Early-Stage Design of Novel Vessels: How can we Take a Step Forward? In *SNAME 14th International Marine Design Conference*, Vancouver, Canada. SNAME.

Charisi, N. D., Kana, A., and Hopman, H. (2022b). Compositional kernels to facilitate multi-fidelity design analysis: Applications for early-stage design. In *AVT-354 Multi-Fidelity Methods for Military Vehicle Design*.

Chaudhuri, A., Peherstorfer, B., and Willcox, K. (2020). Multifidelity cross-entropy estimation of conditional value-at-risk for risk-averse design optimization. *AIAA Scitech 2020 Forum*, 1 PartF.

Di Fiore, F. and Mainini, L. (2024). Physics-aware multifidelity Bayesian optimization: A generalized formulation. *Computers and Structures*, 296:107302.

Drummen, I., Hageman, R. B., and Stambaugh, K. (2022). Multifidelity Approach for Predicting Extreme Global Bending Load Effects. In *9th International Conference on HYDROELASTICITY IN MARINE TECHNOLOGY*, Rome.

Duchateau, E. (2016). *Interactive evolutionary concept exploration in preliminary ship design*. PhD thesis, Technische Universiteit Delft, Delft, the Netherlands.

Duplantier, B. and Rivasseau, V., editors (2018). *Information Theory: Poincaré Seminar 2018*. Birkhäuser.

Duvenaud, D., Lloyd, J. R., Grosse, R., Tenenbaum, J. B., and Ghahramani, Z. (2013). Structure Discovery in Nonparametric Regression through Compositional Kernel Search. *30th International Conference on Machine Learning, ICML 2013*, (PART 3):2203–2211.

Farhang-Mehr, A. and Azarm, S. (2008). On the Entropy of Multi-Objective Design Optimization Solution Sets. *Proceedings of the ASME Design Engineering Technical Conference*, 2:829–838.

Gaggero, S., Vernengo, G., and Villa, D. (2022). A marine propeller design method based on two-fidelity data levels. *Applied Ocean Research*, 123:103156.

Kennedy, M. C. and O'Hagan, A. (2000). Predicting the Output from a Complex Computer Code When Fast Approximations Are Available. *Biometrika*, 87(1):1–13.

Keuning, J. A., van Terwisga, P. F., and Nienhuis, B. (2015). The Possible Application of an AXE Bow on a 5000 Ton Frigate. *SNAME 13th International Conference on Fast Sea Transportation, FAST 2015*.

Krus, P. (2013). Information Entropy in the Design Process. pages 101–112.

Le Gratiet, L. and Garnier, J. (2014). Recursive co-Kriging model for design of computer experiments with multiple levels of fidelity. *International Journal for Uncertainty Quantification*, 4(5):365–386.

Mainini, L., Serani, A., Rumpfkeil, M. P., Minisci, E., Quagliarella, D., Pehlivan, H., Yildiz, S., Ficini, S., Pellegrini, R., Di Fiore, F., Bryson, D., Nikbay, M., Diez, M., and Beran, P. (2022). Analytical Benchmark Problems for Multifidelity Optimization Methods.

Martignon, L. (2001). Information Theory. *International Encyclopedia of the Social & Behavioral Sciences*, pages 7476–7480.

Mavris, D., DeLaurentis, D., Bandte, O., and Hale, M. (1998). A stochastic approach to multi-disciplinary aircraft analysis and design. In *36th AIAA Aerospace Sciences Meeting and Exhibit*, Reston, Virigina. American Institute of Aeronautics and Astronautics.

Molland, A. F. (2008). Chapter 4 - ship structures. In *The Maritime Engineering Reference Book*, pages 116–180. Butterworth-Heinemann, Oxford.

Murphy, K. P. (2012). *Machine learning: a probabilistic perspective*. Cambridge, MA.

Ng, L. W. T. and Willcox, K. E. (2015). Multi-fidelity Monte Carlo Information-Reuse Approach to Aircraft Conceptual Design Optimization Under Uncertainty.

North, D. W. (2017). *Decision Analytic and Bayesian Uncertainty Quantification for Decision Support*, pages 1361–1399. Springer International Publishing, Cham.

Perdikaris, P., Raissi, M., Damianou, A., Lawrence, N. D., and Karniadakis, G. E. (2017). Nonlinear information fusion algorithms for data-efficient multi-fidelity modelling. *Proceedings of the Royal Society A: Mathematical, Physical and Engineering Sciences*, 473(2198).

Rasmussen, C. E. (2003). Gaussian Processes in Machine Learning. *Lecture Notes in Computer Science (including subseries Lecture Notes in Artificial Intelligence and Lecture Notes in Bioinformatics)*, 3176:63–71.

Saad, M. H. and Xue, D. (2023). Initial selection of configurations based on information entropy for multi-level design optimization. *Procedia CIRP*, 119:533–538.

Sapsis, T. P. (2021). Annual Review of Fluid Mechanics Statistics of Extreme Events in Fluid Flows and Waves.

Serani, A., Ficini, S., Grigoropoulos, G., Bakirtzogou, C., Broglia, R., Diez, M., Papadakis, G., Goren, O., Danisman, D. B., Scholcz, T., Hayriye, J. K., Solak, P., and Yıldız, S. (2022). Resistance and Seakeeping Optimization of a Naval Destroyer by Multi-Fidelity Methods. In *AVT-354 Research Workshop on "Multi-Fidelity Methods for Military Vehicle Design"*, Varna.

Shannon, C. E. (1948). A Mathematical Theory of Communication. *Bell System Technical Journal*, 27(3):379–423.

Silver, N. (2012). *The Signal and the Noise: Why So Many Predictions Fail–but Some Don't*. Penguin, New York.

Tupper, E. (2004). 14 - main hull strength. In Tupper, E., editor, *Introduction to Naval Architecture (Fourth Edition)*, pages 276–303. Butterworth-Heinemann, Oxford, fourth edition edition.

Van Oers, B., Takken, E., Duchateau, E., Zandstra, R., Cieraad, S., Van Den Broek De Bruijn, W., and Janssen, M. (2018). Warship Concept Exploration and Definition at The Netherlands Defence Materiel Organisation Introduction: The Netherlands Defence Materiel Organisation. Technical report.

Varley, T. F., Pope, M., Faskowitz, J., and Sporns, O. (2023). Multivariate information theory uncovers synergistic subsystems of the human cerebral cortex. *Communications Biology 2023 6:1*, 6(1):1–12.

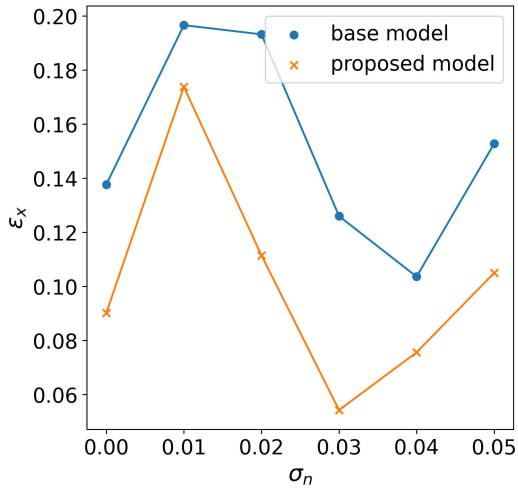

(a) Graph depicting the relationship between ϵ_x and σ_n

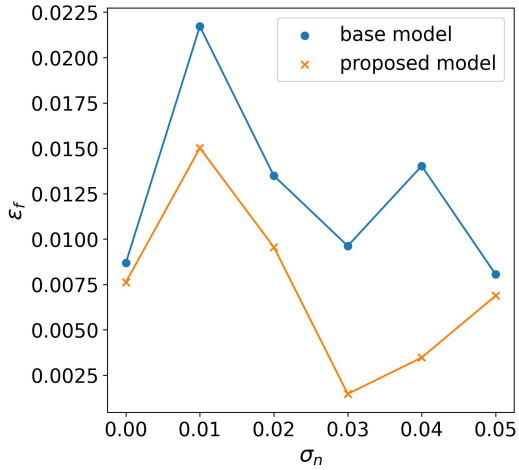

(b) Graph depicting the relationship between ϵ_f and σ_n

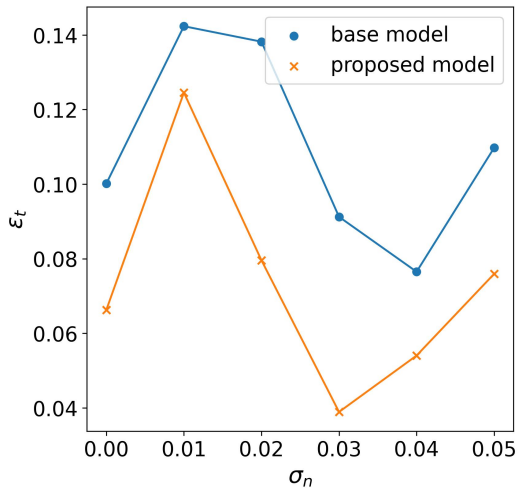

(c) Graph depicting the relationship between ϵ_t and σ_n

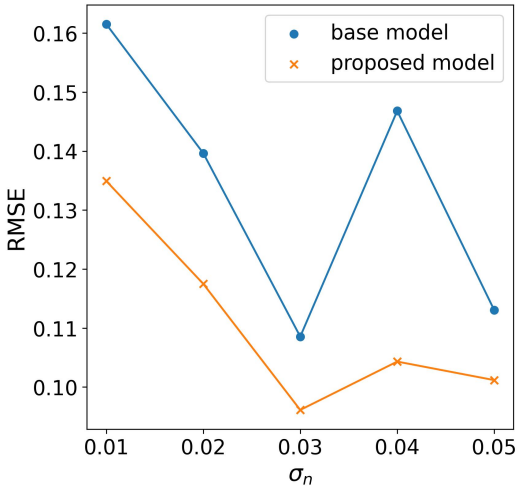

(d) Graph depicting the relationship between $RMSE$ and σ_n

Figure 10: Rastrigin function: Entropy-driven termination criterion, while varying the noise σ_n

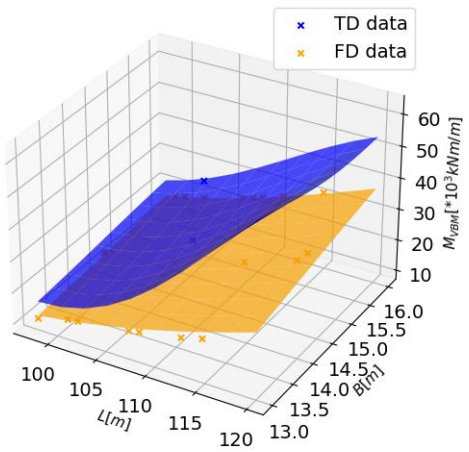

Figure 11: MF design space for the AXE frigates